Journal of Alloys and Compounds 504 (2010) 527–534

Contents lists available at ScienceDirect

Journal of Alloys and Compounds

journal homepage: www.elsevier.com/locate/jallcom

Interfacial and fracture behavior of short-fibers reinforced AE44 based magnesium matrix composites

Bin Hu[a,b], Liming Peng[a,b,*], Bob R. Powell[c], Michael P. Balough[c], Robert C. Kubic[c], Anil K. Sachdev[c]

[a] National Engineering Research Center of Light Alloy Net Forming, Shanghai Jiao Tong University, Shanghai 200240, China
[b] State Key Laboratory of Metal Matrix Composites, Shanghai Jiao Tong University, Shanghai 200240, China
[c] Chemical Sciences and Material Systems Laboratory, General Motors Research & Development Center, Warren, MI 48090, United States

ARTICLE INFO

Article history:
Received 25 February 2010
Received in revised form 25 May 2010
Accepted 29 May 2010
Available online 11 June 2010

Keywords:
Metal-matrix composites (MMCs)
Fracture
Interface
Liquid metal infiltration (LMI)

ABSTRACT

Short fiber reinforced magnesium matrix composite was fabricated by infiltration with molten AE44 (Mg–4.0Al–4.1RE–0.3Mn) alloy. The microstructures in the interfacial region and matrix of composite were characterized using scanning electron microscopy, electron probe micro-analyzer and transmission electron microscope. The fracture initiation and growth was observed by in situ scanning electron microscopy. It was shown that the distribution of the alloying elements was affected by the addition of fibers. The SiO_2 binder in perform reacted with molten magnesium during infiltration, and the reaction product was identified as MgO. The Al–RE phases formed on the surface of fiber and in the matrix, in the form of lamella ($Al_{11}RE_3$) and particle (Al_2RE), respectively. Microcrack initiated in the region of interface of composites, further failure included interfacial debonding add fiber breakage mode or only fiber breakage mode, depending on the fiber distribution to the tensile stress direction.

1. Introduction

In order to reduce the emission of carbon dioxide and greenhouse effect, light weight is of attraction and importance for the automobile industry. As the lightest structural metal, magnesium alloys have already found their widespread applications, especially in power-train systems recently [1,2]. But the low stiffness, low mechanical properties at high temperature and low wear-resistance properties restrict their applications in elevated temperature services. Addition of rare-earth elements (RE) such as Ce and La are known to improve creep resistance and corrosion resistance of Mg–Al base alloys. The AE44 alloy [3,4], which contains 4% Al and 4% RE (mischmetal), has good fracture sensitive mechanical properties such as ductility and strength. These advanced high temperature properties should be attributed to the high content of mischmetal which can stabilize the Al_xRE_y (especially $Al_{11}RE_3$) phase and subsequently suppress the formation of $Mg_{17}Al_{12}$ phase at high temperature.

However, the relatively low stiffness and wear resistance of magnesium alloys (even high RE content in magnesium) still restrict elevated temperature application of Mg alloys in key power-train components. Metal-matrix composites show improved performance than their matrix alloys, such as higher Young's modulus, higher service temperature, improved wear resistance and so on [5,6]. The magnesium matrix composites (Mg-MMCs) can offer potential applications in most severe conditions of automobile power-train to attain the maximum lighten effect, only if they can be approved to own similar overall properties to compete Al-MMCs, with which have already been used in cylinder bores and pistons for decades [7–9]. However, comparing with aluminum-based MMCs, few efforts have been made to study the magnesium-based MMCs [10].

Interface behavior between the matrix and the reinforcement plays an important role in the properties of MMCs [5,6]. The reinforcement type, alloying element, solidification condition and heat-treatment of MMCs can affect the local chemical composition and extent of interfacial reaction of metal-matrix composites [11–16]. Liu et al. [17] have investigated the interfacial reaction in the SiC/Al composites, they have found that the SiO_2 film on the surface of SiC particle was beneficial to improve wettability during infiltration. Rehman et al. [18] have investigated Safimax low-density, standard-density and RF Saffil alumina fibers reinforced magnesium-based composites. The fiber microstructure and porosity were the key features which significantly influence the extent of chemical interaction. There was negligible chemical reaction in composites containing RF-grade Saffil alumina fibers. McMinn et al. [19] have found a reaction zone containing MgO particles at fiber/matrix interface in pure Mg and ZE41 alloy reinforced with

* Corresponding author at: State Key Laboratory of Metal Matrix Composites, Shanghai Jiao Tong University, Shanghai 200240, China. Tel.: +86 21 54742618; fax: +86 21 34202794.
E-mail addresses: hubin.email@gmail.com (B. Hu), plm616@sjtu.edu.cn (L. Peng).

0925-8388/$ – see front matter © 2010 Elsevier B.V. All rights reserved.
doi:10.1016/j.jallcom.2010.05.155

Table 1
Composition (by weight) of the matrix magnesium alloy AE44.

Composition (%)	Al	RE (MM)	Mn	Bal.
Nominal[a]	3.6–4.4	3.6–4.6	0.18–0.50	Mg
Actual	4.0	4.13 (1.7Ce, 2.1La, 0.17Nd, 0.16Pr)	0.27	Mg

[a] Hydro® Magnesium composition.

Table 2
Saffil Preform Used for Casting Mg-MMCs.

Reinforcement	Composition (wt%)	Density (g/cm^3)	Specified fiber (vol%)	Young's modulus (GPa)	Fiber diameter (mean) (μm)
Saffil preform	Fiber: 96–97%Al_2O_3 binder: 3–4%SiO_2	3.3–3.5	15	300–330	3–5

α-Al_2O_3 fibers. They have found that the mean MgO particle size increased with increasing casting temperature. Braszczyńska et al. [20] have investigated the SiCp reinforced pure Mg, and Mg alloys composites. Rare-earth elements based composites exhibited a thick reaction layer of feather-shaped morphology between the matrix and reinforcement, which was related to inhibit the formation of the adhesive bonding between the Mg matrix and SiC particles. Chen et al. [10] have investigated the interfacial behavior of $Mg_2B_2O_5$ whisker-reinforced AZ91D magnesium composite, the effect of interfacial reaction on the $Mg_2B_2O_5$ whiskers was limited, but the interfacial layer was uneven and rough, which may have negative effect on the interfacial bonding. However, no literature reported the interfacial behavior of Saffil fiber reinforced Mg-MMCs which based on the creep-resistant Mg–Al–RE alloys.

The interfacial reaction between fiber and matrix can generate brittle reaction products and decrease effective load transfer from the matrix to the reinforcement, and then deteriorate the strength of the composites [12]. It is necessary to investigate the effect of interfacial reaction on the fracture behavior of the composites. The in situ scanning electron microscope technique (in situ SEM) was used to observe the microcrack nucleation, growth and coalesce in particle or fiber reinforced MMCs [11,21–24]. And it is a qualitatively representative of the fracture behavior to relate the interface behavior to the mechanical properties of the composites, Wang et al. [22] have investigated the fracture behavior of SiCp/AZ91 magnesium matrix composite fabricated by stir casting is investigated using the in situ SEM technique, weak interface and particle segregation have their significant effect on the fracture behavior of composites. Baik [23] has investigated the effect of coating-fiber interfacial reaction on the tensile strength and fracture behavior of squeeze cast 2024Al reinforced with Co-coated alumina fiber. Failure initiation of the composite was entirely by fiber cracking, and further failure induced either interfacial debonding or severe matrix deformation, depending on the interfacial bonding strength. However, there are litter literatures which discussed the fracture behavior of fiber reinforced Mg-MMCs.

Accordingly, the purpose of this work is to study the interfacial behavior of AE44 magnesium alloy based composites reinforced with Saffil fibers. In addition, the crack initiation and growth in composites are also observed and discussed by in situ SEM observations.

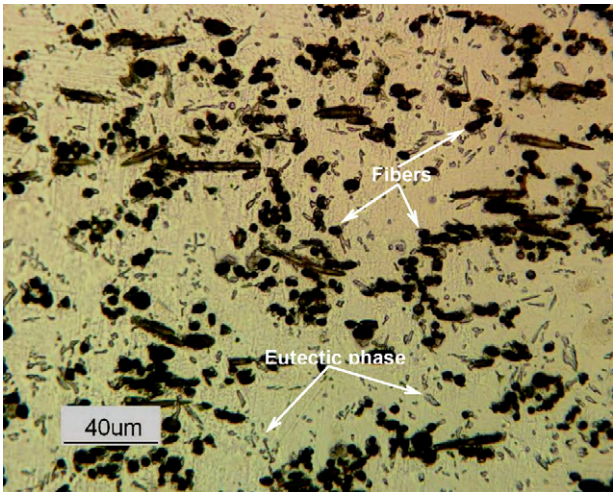

Fig. 2. Optical image microstructures of AE44/Saffil/15_f-F in fiber plane perpendicular to the infiltration direction.

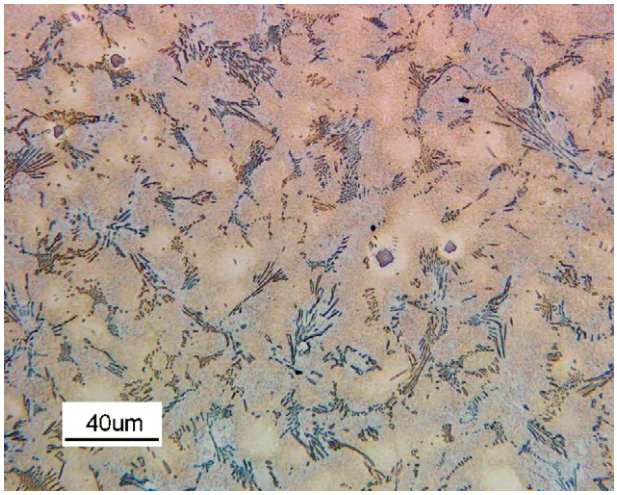

Fig. 1. Optical microstructure of as-squeezed unreinforced AE44 alloy.

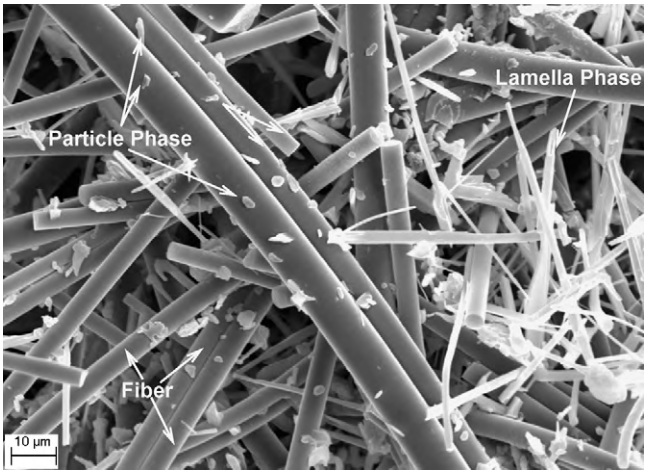

Fig. 3. Morphology of eutectic phase and extracted fibers after deep etching.

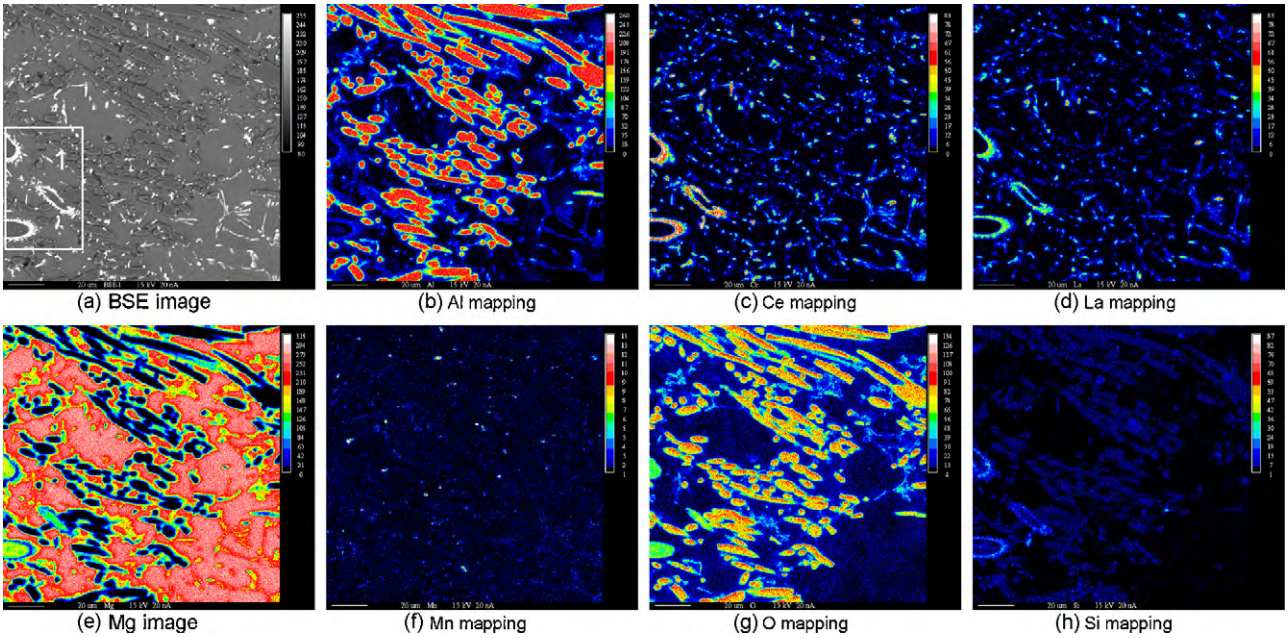

Fig. 4. Electron probe microanalysis mapping of the AE44/Saffil/15$_f$-F composites: (a) back-scattered electron image of alumina binder Saffil reinforced composites; (b) Al mapping image; (c) Ce mapping image; (d) La mapping image; (e) Mg mapping image; (f) Mn mapping image; (g) O mapping image; (h) Si mapping image.

2. Experimental procedures

The creep-resistant magnesium alloy AE44 was adopted as the matrix phase. The AE44 ingots were prepared by remelting pure magnesium alloy, Mg–10 wt%RE, Pure Aluminum alloy and Al–25 wt%Mn alloys. The chemical composition of AE44 ingot from squeezing casting process was measured by inductively coupled plasma-atomic emission spectroscopy (ICP-AES) analysis. The nominal and actual compositions of AE44 are shown in Table 1.

AE44 alloy was infiltrated into the porous, Saffil fiber preforms, reinforcement phase. Thermal Ceramics de France supplied the silica binder RF-grade Saffil fiber preforms as disks, with a size of 105 mm (diameter) × 20 mm (thickness). The disks were 15 vol% solids of fibers. Following the ANSI H35.5 nomenclature for composites, those studied in this work were identified as AE44/Saffil/15$_f$-F, the F indicating that composites were not heat treated. *Note*: The Saffil preforms were manufactured from a wet slurry of cleaned, composite grade ceramic fiber and silica binder. Chemical and physical characteristics of preforms are shown in Table 2. The forming process oriented the fibers into a two-dimensional random planar mat with at least 70% of the fibers parallel to the forming surface.

The composites used in this investigation were fabricated using direct squeeze casting infiltration. The preforms were heated to 800 °C in an external furnace, and then quickly transferred to the cavity (110 mm in diameter and 200 mm in height) in the fixed mold. The mold cavity was preheated to 310 °C. Immediately after insertion of the preforms into the mold cavity, magnesium melt at temperatures 780 °C was poured into the cavity above the preform. A punch was then lowered into the cavity above the melt and preform. It was further lowered (at 10 mm/s) thereby applying pressure to the melt above the preform. The final pressure of 60 MPa was maintained for 2 min until the molten metal was completely solidified. All melting and handling of AE44 were done under an atmosphere of 1 vol% SF6 in CO_2.

The microstructure of the composites and the unreinforced alloy (squeezing casted in the same equipment without preform) were examined by optical microscope (OM) and scanning electron microscopy (SEM using FEI SIRION 200/INCA OXFORD SEM). The matrix alloy and MMC samples were mounted in Lucite (transparent mounting medium), and then were ground using 220, 320, 500, and 800 grit SiC papers and polished using 6 μm and then 1 μm diamond paste. Rinsing at each stage was done with 0.04 μm OPS solution.

Distributions of alloying and reinforcement elements near the fiber were determined by electron probe microanalysis (EPMA) with a Cameca Instruments model SX100 electron probe. Electron beam conditions were typically 15 kV and 40 nA during the analysis.

TEM specimens were cut by diamond wheel and mechanically ground to thickness of 50 μm, and then thinned by the focus ion beam (FIB, by Zeiss NVision-40 CrossBeam Workstation) technique. The observed areas (H-type) for TEM can be selected while the specimens were preparing. A beam of gallium ions operating at 30 kV, and 1.5 μA beam current was used to mill trenches, and polished at a probe current of 50–300 pA. The interface and eutectic phases were investigated using a JEOL2100 transmission electron microscope with an energy dispersion

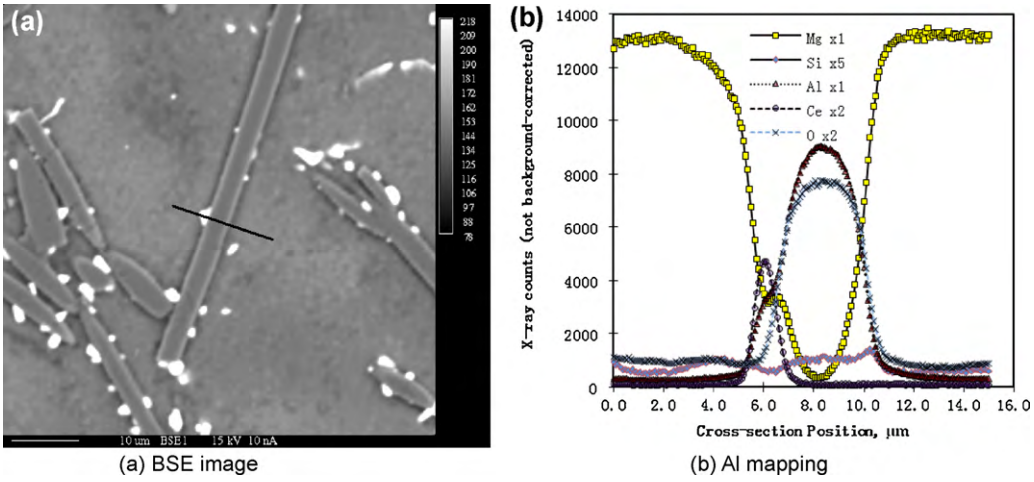

Fig. 5. Electron probe microanalysis line scan across the fibers: (a) line location in AE44/Saffil/15$_f$-F composites; (b) elements content along the scan line.

spectroscopy (EDS) operated at 200 kV, and selected area electron diffraction (SAED).

Mechanical properties of unreinforced alloy and its composite were conducted in Zwick/Roell Z020 tensile machine at a cross-head speed of 1 mm/min using round bar specimens with dimension of 30 mm gauge length and 6 mm diameter. In situ tensile specimens were cut by electric discharge machining (EDM) parallel to the fiber plane with 15 mm gauge length, 5 mm width and 2 mm thickness. The in situ tensile specimens were metallographically polished and gold sputtering, then fixed in mini-tensile loading stage and inserted into the vacuum chamber of SEM. Strain rate was selected at 0.5 mm/min. Tensile loading was applied step by step for direct in situ observation.

3. Experimental results

3.1. Microstructural observations

3.1.1. Optical microstructures

Fig. 1 shows typical optical microstructure of the as-squeezed AE44 alloy, and its composites reinforced with Saffil fibers (Fig. 2). The lamellar phases are distributed in grain boundary region with some particle phases in the unreinforced alloy, as shown in Fig. 1. Eutectic phases in the composite are both close to fibers and in matrix alloy. Fibers remain predominantly in a planar-random arrangement in the composite corresponding to the preform preparation procedure: the preform disks were cut from sheets which had been manufactured by pressing slurries of Saffil fibers, pressing of preform preparing caused the fibers align perpendicular to the pressing direction.

3.1.2. SEM and EPMA observations

In order to observe the morphologies of fibers and the eutectic phases in the squeezing casted composites, magnesium matrix was removed from the composites by "Acetic glycol" etchant for 6 h. The original Al_2O_3 fibers were spliced, as shown in Fig. 3. There is no evidence of fiber damage, which means the infiltration process have not destroyed the preform and fibers. Some phases distribute across different fibers (correspond to the lamella phase in optical images), and small particle shaped phases locate on the surface of fibers. Identification of these phases will be discussed in the following sections.

The distribution of the alloying elements can be delineated by applying the electron probe microanalysis. From the area mapping results in Fig. 4, alloying elements Al, La and Ce tend to segregate both among different fibers, and at the interface between the matrix alloy and the reinforcement (as shown in Fig. 4(b–d)). The element Mn was detected in the (Al, RE)-rich precipitations between fibers. Elements Mg and O were detected in larger size fiber (also called "shot", marked "1"in Fig. 3(a)) without Al, which is related to the penetration of Mg into low-density η-alumina fibers [18]. This kind of low-density alumina fiber contained large amount of porosity, and can totally convert from alumina to magnesia [18]. The line scan of EPMA along the fiber–matrix area of composite shows the distribution of alloying elements of Al and RE near the fiber, as shown in Fig. 5. The silicon was detected both inside and around the fiber in the composites.

The maximum magnification of both OM and regular SEM limited the observation and analysis of small amount of alloying element, such as Si in the composites and morphology of eutectic phases in nano-scale. FIB cutting was used to prepare the TEM specimens, and the magnification in field emission SEM (FE-SEM) can help us to observe clear distribution of the phases and their structures. Fig. 6 shows the microstructure near fiber regions from the TEM sample by FE-SEM. The layer with fine particles distributes between the eutectic phases and fibers, which may be the colloidal binder material used for strengthening the preform during pressure infiltration.

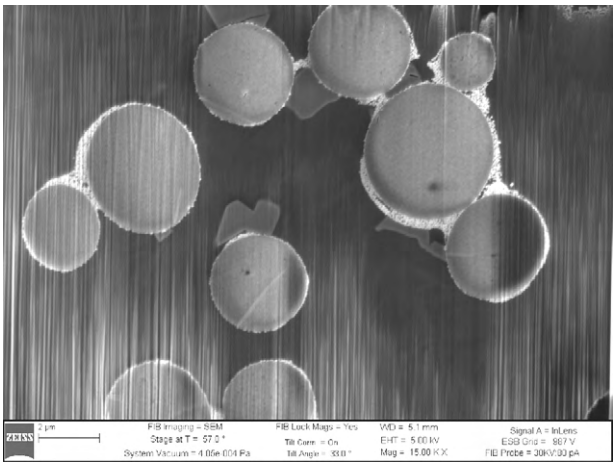

Fig. 6. Back-scattered electron (BSE) images of AE44/Saffil/15_f-F in FIB.

3.1.3. TEM observations

A relatively thick reaction layer with a thickness of 80–100 nm is observed in the interface of composites, as shown in Fig. 7(a). The reaction products are in the form of small particles around the surface of fibers. SAED in interface region shows the characteristics of polycrystalline diffraction pattern, which is identified to be MgO phase based on the calculation of lattice constant.

From the observed area near the fiber, there is a reaction layer isolated all the RE phases, as shown in Fig. 8. The reaction layers have same crystal structure and elements with the reaction zone in Fig. 7(a), which was also identified to be the MgO phase. And the particle phase is identified to be the Al_2RE base on the elements and lattice diffraction analysis.

The atomic content of element Si in region 4 is only 0.91% (as shown in Table 3), which is even lower than the Al_2O_3 fiber. The reaction can be speculated that it is occurred between the SiO_2 binder and magnesium melt. The mapping image in Fig. 9(b) shows no Al was detected in region 4, which also confirmed that the reaction region between the fiber and Al_2RE phase occurred by the SiO_2 binder with Mg melt.

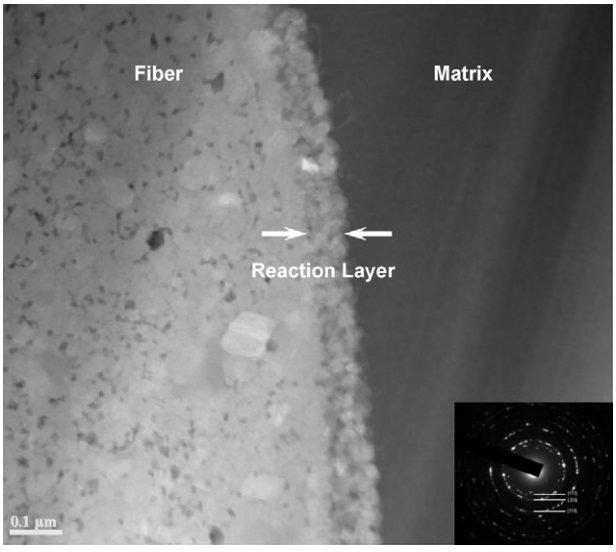

Fig. 7. TEM image showing the interfacial microstructure in AE44/Saffil/15_f-F composites, and the selected area diffraction patterns for interfacial reaction zone (identified to be MgO).

Table 3
Elements analysis in selected region in Fig. 8 (at.%).

Position	Al	Ce	La	Si	O	Mg
1	63.6	25.16	11.24	–	–	–
2	3.84	–	–	0.29	–	95.87
3	37.75	–	–	1.34	58.85	2.06
4	2.39	–	–	0.91	42.51	54.19

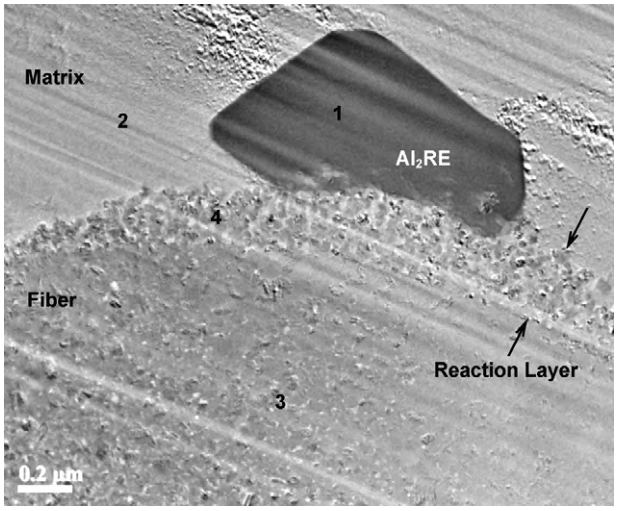

Fig. 8. Transmission electron micrograph of AE44/Saffil/15$_f$-F composites in the interface region.

Fig. 10 shows the lamella phase in the matrix of composite among fibers and its selected area electron diffraction pattern. The lamella phase was identified to be the $Al_{11}RE_3$ phase, which has the same phase identification with the AE series magnesium alloys [3,4].

Table 4
Mechanical properties of the as-cast AE44/Saffil/15$_f$-F composite and AE44 alloy.

	UTS (MPa)	YS (MPa)	El. (%)	E (GPa)
AE44 matrix	197.69	98.05	10.26	43.6
AE44/Saffil/15$_f$-F	221.62	163.26	1.28	72.3

3.2. Mechanical properties

The mechanical properties of as-cast AE44 alloy and its composites are shown in Table 4. The tensile properties were improved by incorporating of Saffil fibers, e.g., the yield strength (YS) of composite is 66.5% better than its matrix alloy. However, the elongation (El.) to failure decreased significantly.

3.3. Microcrack observations

Fig. 11 shows the morphology evolution of the near-notch region during the crack initiation and growth in the composites. Two fibers, marked region "1" and "5", represent roughly perpendicular and parallel distributing direction to the tensile direction, respectively. The crack is initiated in the tip of fiber in region "1". This indicate that microcrack is mainly nucleated by interface decohesion of fibers, which arrayed perpendicular to tensile direction. With increasing in applied load, microcracks grew and new microcracks were nucleated elsewhere, as shown in region "2", "3" and

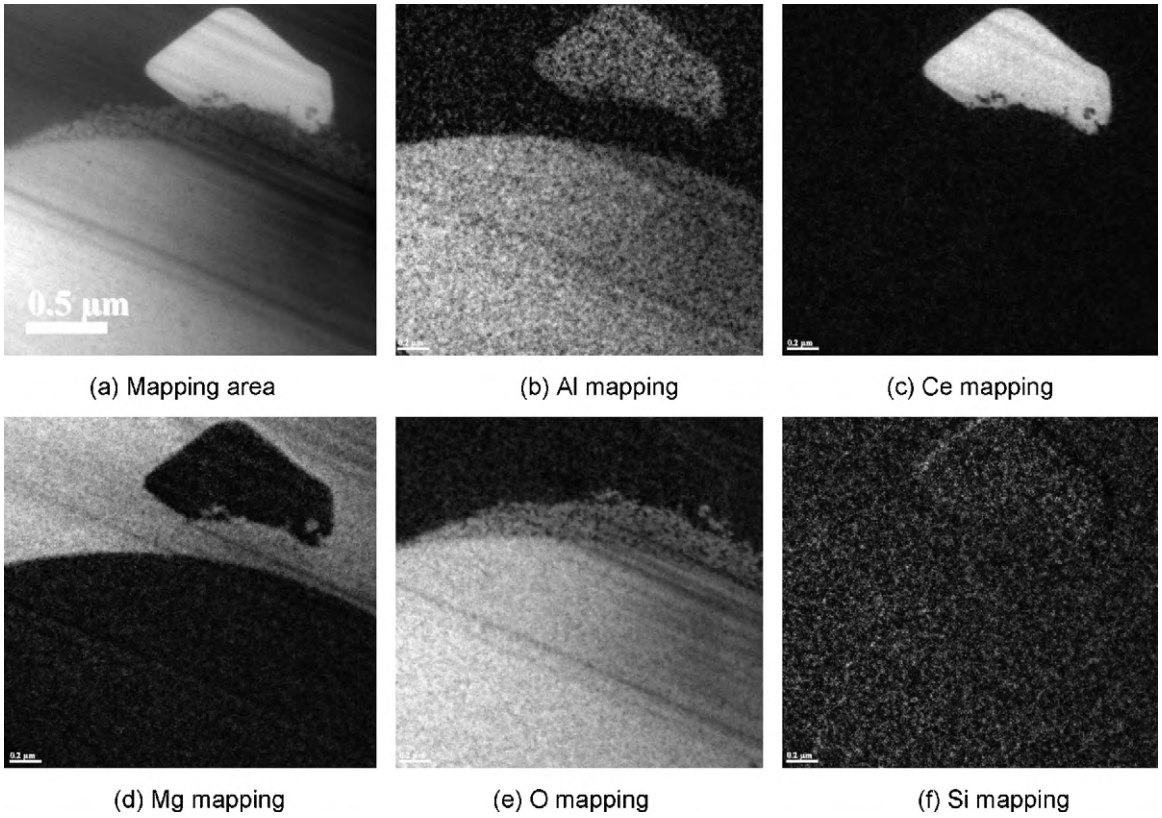

Fig. 9. EDS scan of the interface area in Fig. 8: (a) mapping area; (b) Al mapping; (c) Ce mapping; (d) Mg mapping; (e) O mapping; (f) Si mapping.

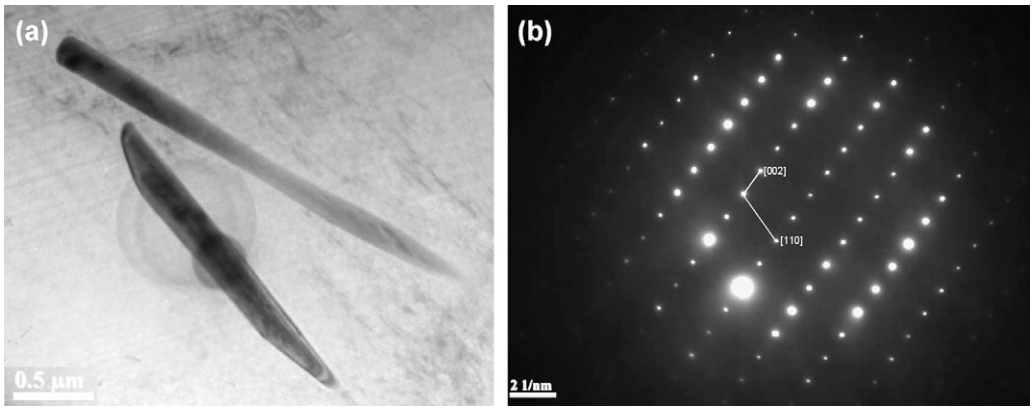

Fig. 10. Lamellar phase among the fibers: (a) morphology of lamellar phase; (b) SAED pattern of lamellar phase.

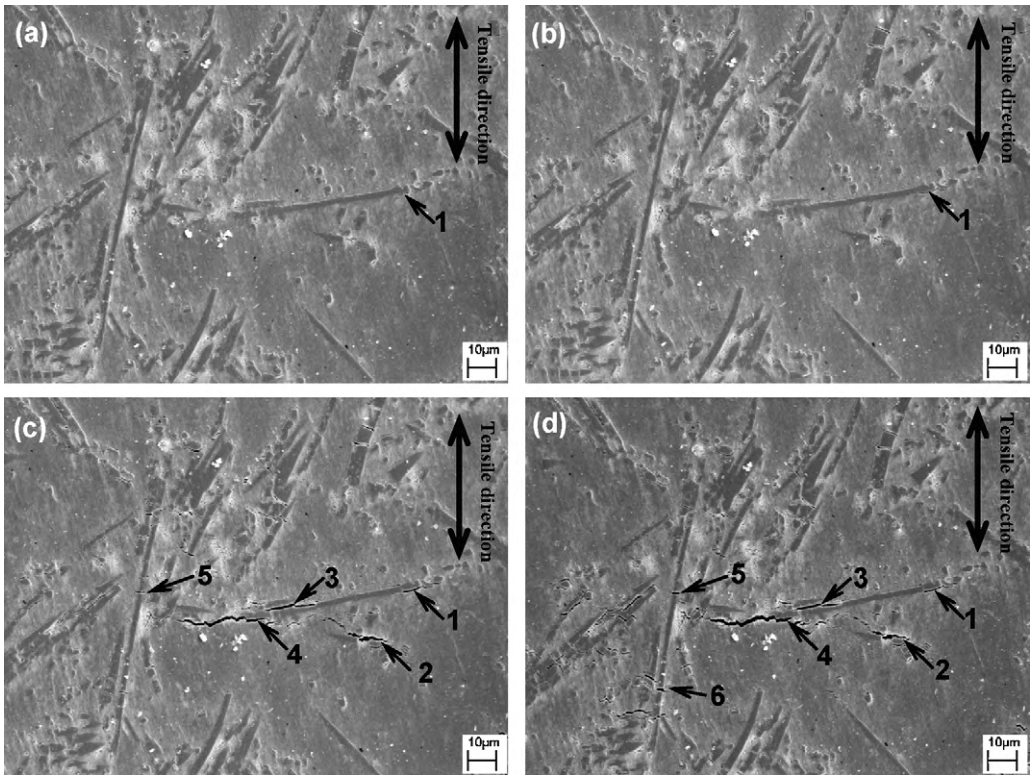

Fig. 11. In situ SEM images of the crack growth in AE44/Saffil/15_f-F composites, at loading stress of: (a) 1805 N (~187.4 MPa); (b) 1855 (192.6 MPa); (c) 1902 (~197.5 MPa); (d) fractured.

"4" of Fig. 11(c). The crack in region "3" between two fibers also can be identified in Fig. 11(c and d).The binder agents (SiO_2) are easy to distribute in the fiber/fiber region, which can be transformed to MgO during the infiltration or solidification. So, it is easy to act as crack initiation and propagation path.

As shown in Fig. 11(c and d), fiber breakage in region "5" can be observed, which is caused by the growth of crack in region "4". This fiber is arrayed parallel to tensile direction, more load transfer to the reinforcement as compared with that of fiber in region "1". Another crack in region "6" is observed, which indicate that main contribution of the improved strength can be ascribed to load transfer to the fibers which are parallel to tensile direction.

4. Discussion

Solidification inside the preheated preform is relatively slow due to high preheated temperature of preform (800 °C) and high pouring temperature (780 °C). The enrichment of alloying elements occurs at the final stage of solidification. Therefore, the matrix grain size of the composites is relatively coarser than the unreinforced alloy by same squeezing casting procedure. The eutectic phases can be found both on the surface of the fiber and between different fibers, as showed in Fig. 3. According to the Al–Ce phase diagram [25], the $Al_{11}Ce_3$ phase is formed prior to Al_2Ce phase during solidification. The lamella $Al_{11}RE_3$ phase and the blocky Al_2RE phases were observed among the fibers and in the surface of the fiber, respectively, which indicates that the solidification started at locations away from the fibers (inter-fiber region) and finished in the surface of the fibers. Similar observations have been made in Al and Mg composites [26] reinforced with Saffil. The preform temperature in the process of aluminum matrix composites is always from 200 to 400 °C. However, the magnesium alloys are flammable at high temperature, even under protective gas when transferred from furnace to cavity of squeezing casting dies. In order to reduce

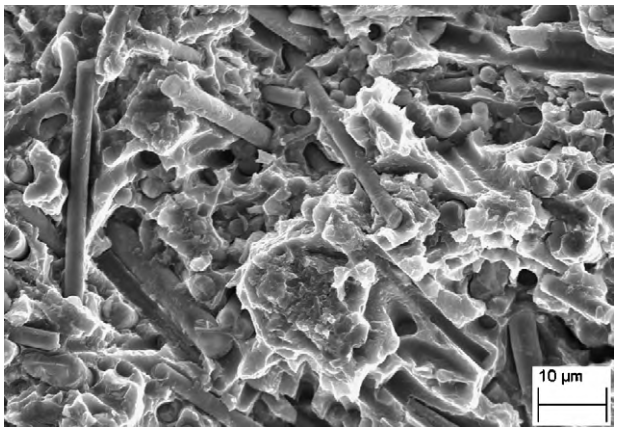

Fig. 12. SEM images of the fracture surface in AE44/Saffil/15_f-F composites.

the operational temperature of Mg, we use higher preform temperature to attain sound infiltration process [27].

The Gibbs free energies of reaction for the proposed reduction reactions at the interface, at the infiltration temperature, 780 °C (953 K), favor reduction of the oxides magnesium [28,29]. Al_2O_3 fibers and colloidal SiO_2 binder are the materials of preform, which can be reacted with molten Mg at different reaction kinetics, they are shown below:

$$Mg + \tfrac{1}{3}Al_2O_3 \rightarrow MgO + \tfrac{2}{3}[Al] \quad \Delta G_{1000\,K} = -39\,kJ \tag{1}$$

$$Mg + \tfrac{1}{2}SiO_2 \rightarrow MgO + \tfrac{1}{2}[Si] \quad \Delta G_{1000\,K} = -128\,kJ \tag{2}$$

The binder material was in the form of powder/particle on the surface of the fiber, as shown in Fig. 6. The element of Si was detected near the fiber by EPMA (Fig. 5) and EDS of TEM (Table 3), Si in position 4 (0.91, SiO_2 binder region before infiltration) had higher content than that in position 2 (0.29, in AE44 matrix).

The thick MgO layer in the fiber/matrix interface of composite undoubtedly has their inverse effect on the fracture behavior and mechanical properties, as shown in Table 4. The weak interface cannot withstand the stress from the matrix, and microcrack is prone to initiate in the interfacial region, as shown in regions "1" to "4" of Fig. 11.

The in situ SEM observation was a free surface phenomenon, which may not be representative failure behavior within the bulk of specimen. The fractography was used to validity the above explanation. Fig. 12 shows the tensile fracture surfaces of the composite. The fracture surface of composite contains exposed fibers which had a relatively clean, smooth surface. And the pull-out fibers and deep voids are frequently observed. These indicate that the interfacial bonding strength was not high enough for the composite during transferring load from matrix to the fibers. The binder material deteriorates some of the strength of the composites, which need to choose a better binder agent of the perform for the magnesium matrix composites.

Sohn et al. [21] have also used in situ SEM technique to investigate the fracture behavior of fiber/whisker-reinforced Mg composite. They found that the microcracks were initiated at the reinforcement/matrix interface. But Baik [23] suggested that the initial failure of fiber occurred by fiber cracking in cobalt-coated alumina fiber reinforced aluminum composites, and then further failure include either fiber debonding or severe matrix deformation, depend on interfacial bonding strength. In this study, no evidence of fiber breakage was found in as-squeeze composite (Fig. 3) even under relative high load applied (Fig. 12). Crack initiation in AE44/Saffil/15_f-F composite is nucleated in the interface regions, including fiber/matrix and fiber/fiber regions, which indicate the interfacial reaction between SiO_2 binder and magnesium matrix deteriorated the mechanical properties and elongation of the investigated composite.

5. Conclusions

The study on the interfacial reaction and fracture behavior of Mg-MMCs fabricated by squeezing casting infiltration using OM, TEM, EMPA and in situ SEM reveals the following:

1. Mechanical tensile strength of AE44 alloy can be improved by incorporating Saffil fibers. The rare-earth alloying elements, such as Ce and La are distributed at the interface in the form of Al_2RE particle phase on the surface of fiber, and $Al_{11}RE_3$ lamellar phase in the matrix.
2. The reaction product MgO was identified in the interface region of composites, which is the reaction product between silica binder and Mg melt during infiltration on the surface of fibers.
3. The fracture mechanism of Mg-MMCs was controlled by fiber/matrix interface and fiber breakage. Microcrack initiated in the region of interface of composites, further failure included interfacial debonding adding fiber breakage mode or only fiber breakage mode, depending on the fiber distribution to the tensile stress direction.

Acknowledgements

The authors would like to thank Alan. Luo (GMRD) for many insightful discussions regarding microstructure and properties of the matrix alloy and composites. In addition the kindly assistance of our colleagues at SJTU, Yanling Yang, Zhen Zhao and Ming Sun, during the preparation and testing of the materials is gratefully appreciated. This work was sponsored by General Motors R&D, Key Basic Research Foundation of the Shanghai Committee of Science and Technology (08JC1411400) and National High Technology Research and Development Program of China (863 Program no. 2009AA033501).

References

[1] H. Friedrich, S. Schumann, J. Mater. Process. Technol. 117 (2001) 276–281.
[2] A. Luo, Int. Mater. Rev. 49 (2004) 13–30.
[3] P. Bakke, H. Westengen, in: N.R. Neelamegham, H.I. Kaplan, B.R. Powell (Eds.), Magnesium Technology, TMS, Warrendale, PA, 2005, pp. 291–296.
[4] S.M. Zhu, M.A. Gibson, J.F. Nie, M.A. Easton, P. Bakke, in: Mihriban O. Pekguleryuz, Neale R. Neelameggham, Randy S. Beals, Eric A. Nyberg (Eds.), Magnesium Technology, TMS, Warrendale, PA, 2008, pp. 437–442.
[5] K.U. Kainer, Metal Matrix Composites, Wiley-VCH, Weinheim, Germany, 2006.
[6] N. Chawla, K.K. Chawla, Metal Matrix Composites, Springer, New York, USA, 2006.
[7] T. Takami, M. Fujine, S. Kato, H. Nagai, A. Tsujino, Y.H. Masuda, SAE paper, No. 2000011231, 2000.
[8] T. Donomoto, N. Miura, K. Funatani, N. Miyake, SAE Technical paper, No. 830552.1983.
[9] N. Chawla, K.K. Chawla, J. Miner. Met. Mater. Soc. 58 (2006) 67–70.
[10] S.H. Chen, P.P. Jin, G. Schumacher, N. Wanderka, Compos. Sci. Technol. 70 (2010) 123–129.
[11] B.L. Mordike, P. Lukáč, Surf. Interface Anal. 31 (2001) 682–691.
[12] Y.D. Huang, N. Hort, H. Dieringa, K.U. Kainer, Y.L. Liu, Acta Mater. 53 (2005) 3913–3923.
[13] W.B. Xue, Q. Jin, Q.Z. Zhu, M. Hua, Y.Y. Ma, J. Alloys Compd. 482 (2009) 208–212.
[14] J. Hu, X.F. Wang, S.W. Tang, Compos. Sci. Technol. 68 (2008) 2297–2299.
[15] P. Rodrigo, P. Poza, V. Utrilla, A. Ureña, J. Alloys Compd. 479 (2009) 451–456.
[16] B.W. Xiong, Z.F. Xu, Q.S. Yan, C.C. Cai, Y.H. Zheng, B.P. Lu, J. Alloys Compd. 497 (2010) L1–L4.
[17] J.W. Liu, Z.X. Zheng, J.M. Wang, Y.C. Wu, W.M. Tang, J Lü, J. Alloys Compd. 465 (2008) 239–243.
[18] F.U. Rehman, S. Fox, H.M. Flower, D.R.F. West, J. Mater. Sci. 29 (1994) 1636–1645.
[19] A. McMinn, R.A. Page, W. Wei, Metall. Mater. Trans. 18A (1987) 1073–5623.
[20] K.N. Braszczyńska, L. Lityńska, A. Zyska, W. Baliga, Mater. Chem. Phys. 81 (2003) 326–328.
[21] K.S. Sohn, K. Euh, S. Lee, I. Park, Metall. Mater. Trans. 29A (1998) 2543–2554.

[22] X.J. Wang, K. Wu, W.X. Huang, H.F. Zhang, M.Y. Zheng, D.L. Peng, Compos. Sci. Technol. 67 (2007) 2253–2260.
[23] K.H. Baik, Mater. Sci. Eng. 355A (2003) 79–87.
[24] R. Tavangar, L. Weber, A. Mortensen, Mater. Sci. Eng. 395A (2005) 27–34.
[25] K.A. Gschneidner Jr., F.W. Calderwood, Binary Alloy Phase Diagrams (1988) 2–43.
[26] A. Mortensen, V.J. Michaud, J.A. Cornie, M.C. Flemings, L. Masur, ASM Conference Proceedings, ASM International, Metals Park, OH, 1988, pp. 7–13.
[27] B. Hu, L. Peng, B. Powell, A. Sachdev, in: Sean Agnew, A. Eric, Nyberg, Wim Sillekens, R. Neale, Neelameggham (Eds.), Magnesium Technology 2010, TMS, Seattle, WA, 2010, pp. 473–480.
[28] Europe SGT.DGTE Substance Database at KTH, 1989.
[29] G.H. Cao, Z.G. Liu, J.M. Liu, G.J. Shen, S.Q. Wu, Compos. Sci. Technol. 61 (2001) 545–550.